Synoptic versus orographic control on stationary convective banding

Article

Barrett, A. I., Gray, S. L. ORCID: https://orcid.org/0000-0001-8658-362X, Kirshbaum, D. J., Roberts, N. M., Schultz, D. M. and Fairman Jr, J. G. (2015) Synoptic versus orographic control on stationary convective banding. Quarterly Journal of the Royal Meteorological Society, 141 (689). pp. 1101-1113. ISSN 1477-870X doi: 10.1002/qj.2409 (Part B) Available at https://centaur.reading.ac.uk/37572/

RMetS
Royal Meteorological Society

Synoptic versus orographic control on stationary convective banding

Andrew I. Barrett,[a]* Suzanne L. Gray,[a] Daniel J. Kirshbaum,[b] Nigel M. Roberts,[c] David M. Schultz[d] and Jonathan G. Fairman, Jr[d]

[a]*Department of Meteorology, University of Reading, UK*
[b]*Department of Atmospheric and Oceanic Sciences, McGill University, Montreal, Quebec, Canada*
[c]*MetOffice@Reading, University of Reading, UK*
[d]*Centre for Atmospheric Science, School for Earth, Atmospheric and Environmental Sciences, University of Manchester, UK*

*Correspondence to: A. I. Barrett, Department of Meteorology, University of Reading, Reading RG6 6BB, UK.
E-mail: a.i.barrett@reading.ac.uk

Quasi-stationary convective bands can cause large localised rainfall accumulations and are often anchored by topographic features. Here, the predictability of and mechanisms causing one such band are determined using ensembles of the Met Office Unified Model at convection-permitting resolution (1.5 km grid length). The band was stationary over the UK for 3 h and produced rainfall accumulations of up to 34 mm. The amount and location of the predicted rainfall was highly variable despite only small differences between the large-scale conditions of the ensemble members. Only three of 21 members of the control ensemble produced a stationary rain band; these three had the weakest upstream winds and hence lowest Froude number. Band formation was due to the superposition of two processes: lee-side convergence resulting from flow around an upstream obstacle and thermally forced convergence resulting from elevated heating over the upstream terrain. Both mechanisms were enhanced when the Froude number was lower. By increasing the terrain height (thus reducing the Froude number), the band became more predictable.

An ensemble approach is required to successfully predict the possible occurrence of such quasi-stationary convective events because the rainfall variability is largely modulated by small variations of the large-scale flow. However, high-resolution models are required to accurately resolve the small-scale interactions of the flow with the topography upon which the band formation depends. Thus, although topography provides some predictability, the quasi-stationary convective bands anchored by it are likely to remain a forecasting challenge for many years to come.

Key Words: orography; convection; predictability; rainband; convective-scale ensembles; elevated heating; lee convergence

Received 17 December 2013; Revised 15 May 2014; Accepted 4 June 2014; Published online in Wiley Online Library

1. Introduction

The largest precipitation accumulations occur where the rainfall rate is highest for the longest time (Doswell *et al.*, 1996). Quasi-stationary convection produces high rainfall rates in long-duration events and is therefore often associated with flooding. Stationary convective rainbands are a common mode of convection over elevated terrain (e.g. Cosma *et al.*, 2002; Kirshbaum *et al.*, 2007) and can remain anchored over or near a particular topographic feature. Changes of surface roughness and heating at the coast can also produce circulations that result in large rainfall accumulations from quasi-stationary convection (Warren *et al.*, 2014). Quasi-stationary lines of convection can cause flash flooding (e.g. Golding, 2005), especially when the rain from such systems falls on terrain with steep valleys that can further focus the large volumes of rain water into a smaller region. It is therefore important to understand under what conditions these topographically driven stationary convective rainbands form, what mechanisms are involved in their maintenance and how predictable they are.

Stationary convective bands have been observed over various mountain ranges. For example, bands have been recorded over Japan (Yoshizaki *et al.*, 2000), the Massif Central in France (Miniscloux *et al.*, 2001; Cosma *et al.*, 2002) and the Coastal Range,

Oregon, USA (Kirshbaum and Durran, 2005). Similar quasi-stationary banded convection is also reported in Schumacher *et al.* (2010) in the lee of the Rockies in central USA, and non-stationary embedded convective bands have been reported over the German Alps (Langhans *et al.*, 2011).

The climatology of precipitation can be affected by repeated occurrences of stationary banded precipitation. Godart *et al.* (2011) reported that orographic banded convection can contribute up to 40% of the seasonal rainfall total in some regions of southern France. Similarly, Miniscloux *et al.* (2001) report that banded rainfall is important in seasonal totals, despite the bands typically having lower intensities than individual non-stationary cells.

The terrain can disturb the flow in two ways: by mechanically deflecting the air over or around it and by acting as an elevated heat source. Bands can result from mechanical deflection when the air stream splits into two upon encountering an obstacle such as is observed around the Olympic mountains (Mass, 1981) and over Portland, Oregon (Yuter *et al.*, 2011)–both in the northwest USA. Such deflection can result in a convergence zone setting up in the lee of the terrain (such as the Puget Sound Convergence Zone in Mass, 1981) which helps focus convection initiation to a small region. In the right flow conditions, repeated initiation at one location can result in a band forming downwind. The likelihood of deflection around an obstacle in the flow (rather than air flowing over it) is predicted by the Froude number

$$Fr = \frac{U}{Nh}, \tag{1}$$

where U is the wind speed, N is the Brunt–Väisälä frequency and h is the representative height of the terrain. For $Fr < 1$, flow is likely to be deflected around the terrain and for $Fr > 1$ air is likely to flow over the terrain.

Small-scale topographic perturbations on a large-scale mountain have also been found to be important in initiating convective bands. These bands can result from lee-side convergence around the smaller terrain obstacles (Cosma *et al.*, 2002). This mechanism is similar to that described in Mass (1981) but on a much smaller scale. Alternatively, if stably stratified flow ascends a terrain feature rather than detouring around it, the small-scale terrain features produce lee waves that can anchor convective bands. Once the air has ascended far enough up the large-scale orography to produce a cap cloud, a convective band can be formed if the phase of the lee-wave interacts favourably with the leading edge of the cap cloud and gives sufficient vertical velocities to release the conditional instability present (Kirshbaum *et al.*, 2007; Fuhrer and Schär, 2007).

Convection initiation can also result from solar heating of the elevated terrain, which heats up more during the day than the surrounding air at the same vertical level. This heating can modify the circulation over and downstream of the terrain (Crook and Tucker, 2005). The resulting baroclinic environment can generate upslope flow over the mountain or a band of ascent downwind (Kirshbaum, 2013). Elevated heating can enable flow to pass over the terrain when it would otherwise be deflected around it (Reisner and Smolarkiewicz, 1994). Furthermore, modifications to cloudiness and heating around the terrain obstacle can be important; for an event in the UK, Lean *et al.* (2009) reported that surface heating beneath a small hole in a cloud layer to the lee of high ground was an important factor in thunderstorm development farther downstream. Although elevated heating is thus an effective mechanism for convection initiation, its potential for generating stationary convective bands has not been examined.

In this study, a convection-permitting ensemble is used to investigate a stationary convective band that formed over the UK on 27 August 2011. This case was selected for study because it was the longest lasting stationary orographic band with the largest rainfall accumulation over the UK in the 18 months prior to summer 2012 (the period of the available archived model data). The band is not exceptional in terms of the rainfall produced, but its long duration is typical of high-impact rainfall events over the UK (e.g Golding, 2005; Warren *et al.*, 2014).

A convection-permitting ensemble is used, similar to that routinely run by the Met Office. Convection-permitting models better represent both the convective processes and the variable topography related to their initiation. However, model verification becomes difficult at high resolution as traditional measures of skill (e.g. root-mean-square difference) decrease as model resolution increases (Baldwin *et al.*, 2001; Roebber *et al.*, 2004) despite the predicted rainfall distributions looking more realistic. The main reason for this is the greater potential to misplace the rainfall features in models with more grid points, resulting in penalization for both a false alarm and a miss (the 'double-penalty' problem). As a consequence, new measures of forecast skill have been developed (e.g. Wernli *et al.*, 2008; Roberts and Lean, 2008) which verify the model by comparing the statistics of the rainfall field with those from observations. Using these methods, high-resolution models have been shown to be generally more skilful than coarse-resolution models (Mass *et al.*, 2002; Roberts and Lean, 2008; Roberts *et al.*, 2009; Kendon *et al.*, 2012; Mittermaier *et al.*, 2013), although Zhang *et al.* (2006) demonstrate that this is not necessarily true of individual cases.

The timing and location of convective initiation is sensitive to the initial conditions of the model, and for that reason we use an ensemble approach to determine how sensitive convective bands are to these conditions. Clark *et al.* (2009) found convection-permitting ensembles to be beneficial over ensembles of coarser resolution with parametrized convection, even when the size of the ensemble has to be small due to limited computing resources. The ensemble approach allows us to determine the predictability of these potentially high-impact events, as well as to determine the mechanisms through which they form. Similar methodologies were used in Hanley *et al.* (2011, 2013) who found that orographic and frontal convection was highly sensitive to small uncertainties in the larger-scale flow. In this study, we examine the synoptic variability and also perturb the surface properties within the simulations (terrain height and albedo) to establish the relative importance of different physical processes.

A description of the case studied is presented in section 2 followed by an overview of the model used for analysis in section 3. Analysis of the control ensemble is presented in section 4 and the effect of changing the terrain specification is assessed in section 5. Section 6 contains analysis of experiments designed to separate mechanical and thermal effects of the terrain. Section 7 concludes this article.

2. Case description: 27 August 2011

A stationary convective rainband, approximately 25 km wide by 100 km long, formed over the Yorkshire Dales region of Northern England (Figure 1) and produced locally heavy and sustained rainfall. The band formed across an area of elevated terrain, just downwind of the Lake District and along a ridge of the Yorkshire Dales. The band was stationary for 3 h during which it produced a maximum radar-derived rainfall accumulation of 34 mm (Figure 2). Much of the area around the band received little or no rain; however, a large portion of the area under the band received more than 8 mm of rain in 3 h.

The rainfall totals shown in Figure 2 were derived from 5 min radar data from the UK 1 km radar network (Harrison *et al.*, 2009, 2012). Several difficulties exist in accurately determining rainfall rates over elevated terrain using radar, for example partial blockage of the radar beam by hills between the radar and the rainfall or spurious returns from ground clutter. These artefacts can sometimes appear similar to stationary rainfall; however, manual inspection of the radar data and comparison with surface rain gauges and satellite data (not shown) indicate that this band was present, although the precise rainfall amounts are subject to some uncertainty.

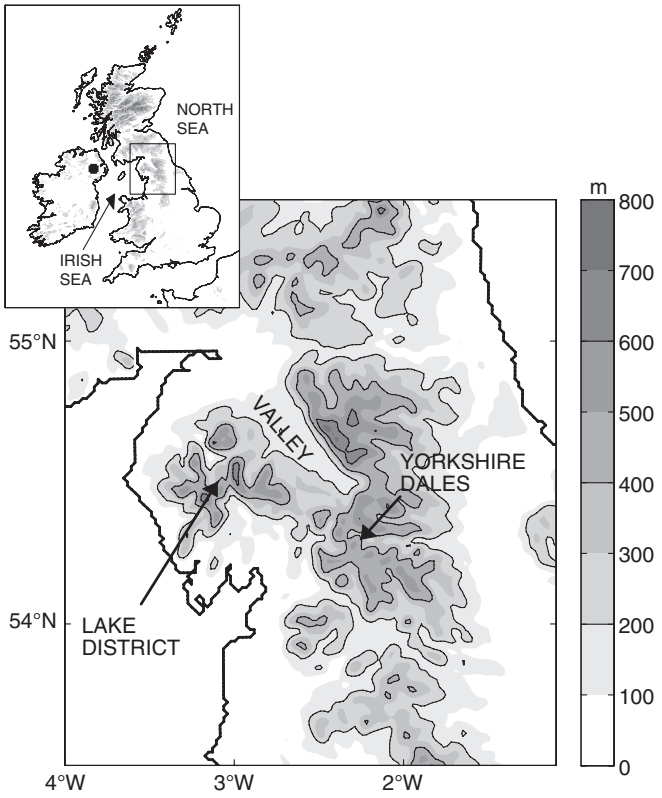

Figure 1. Map of terrain heights from the Unified Model at 1.5 km grid-spacing, with labels showing the Lake District, the Yorkshire Dales and a valley that is referred to in the text. The dot marked on the inset figure shows the location of the Castor Bay radiosonde site.

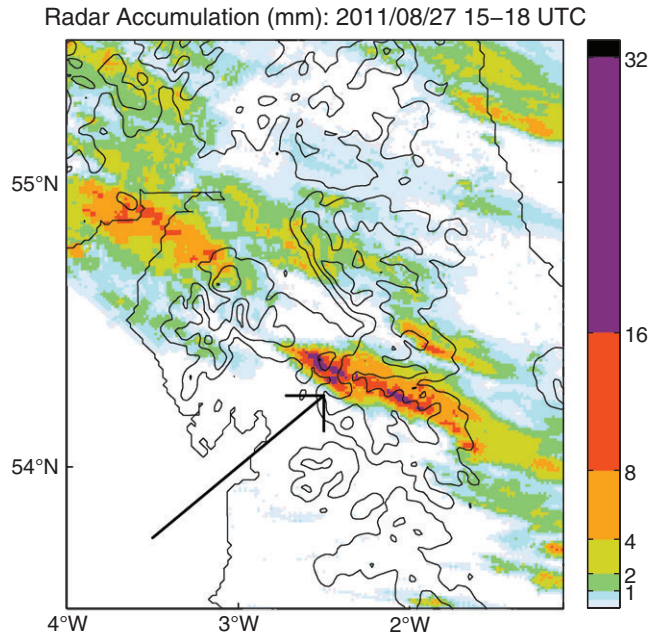

Figure 2. Three hour rainfall accumulations (mm) from the Met Office radar network from 1500 to 1800 UTC. The UK coastline and the terrain elevation contours every 200 m are shown in black. The band of interest is marked by the black arrow.

The band formed within the southwest quadrant of a slow-moving, decaying low pressure system. The synoptic chart at 1200 UTC 27 August 2011 (Figure 3), about 3 h before the band formed, shows the low pressure centre to the northeast of the UK. This synoptic set-up brought northwesterly flow to northwest England (the band formation region). The low pressure system was slow-moving, hence the synoptic situation did not change during the period of interest.

The only radiosonde launch reasonably close in time and space to the convective band was from Castor Bay, Northern

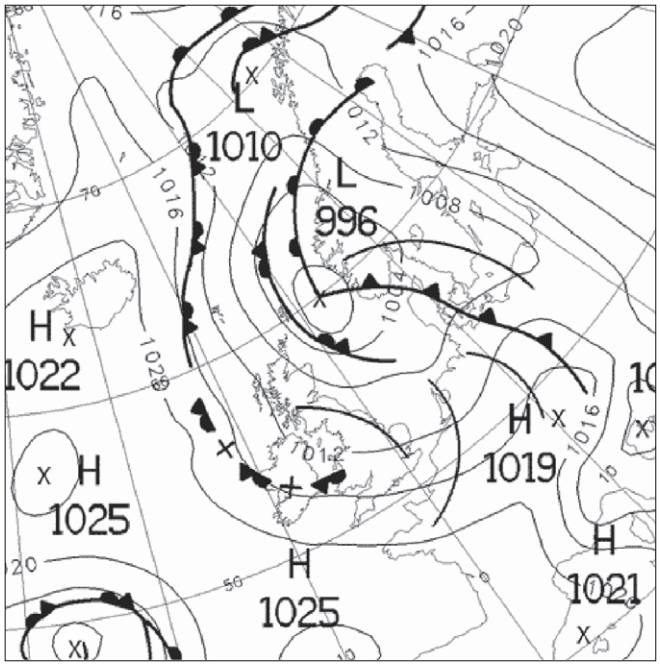

Figure 3. Met Office synoptic analysis at 1200 UTC 27 August 2011, approximately 3 h before the band formed. © Crown copyright, Met Office.

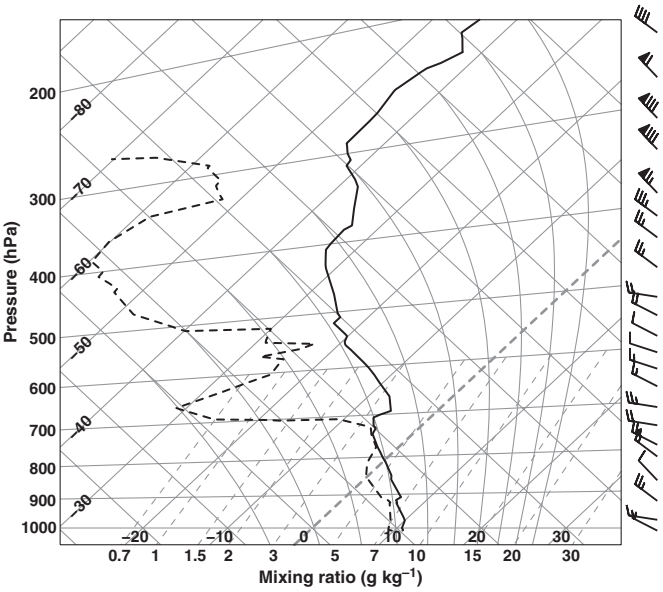

Figure 4. Tephigram plot from radiosonde ascent at Castor Bay, Northern Ireland, at 1200 UTC 27 August 2011. Data obtained from University of Wyoming, http://weather.uwyo.edu/upperair/sounding.html (accessed 16 June 2014).

Ireland, at 1200 UTC 27 August 2011 (Figure 4). Because Castor Bay lies upstream of the Irish Sea (Figure 1) and did not experience any convective precipitation on this day, its local environment is likely less supportive of convection than that over and downwind of the Lake District. Nevertheless, it provides useful observational insight into the regional stability, moisture, and wind profiles. The sounding shows a shallow and moist boundary layer overlain by a weakly conditionally unstable layer, capped by an inversion just above the freezing level. Although the sounding contains no Convective Available Potential Energy (CAPE), its near moist-neutrality below 700 hPa suggests that even marginal diurnal heating would be sufficient to create moist instability.

3. Model description and set-up

The most recently released version of the Met Office Unified Model (MetUM) at the time of this study (vn 7.8) was used for the

numerical simulations. The MetUM is used operationally by the Met Office for weather forecasting on domains ranging from the entire globe to limited-area domains just encompassing the UK (Brown *et al.*, 2012). The MetUM solves non-hydrostatic, fully compressible deep-atmosphere equations of motion using semi-implicit, semi-Lagrangian time integration (Davies *et al.*, 2005). An Arakawa C grid is used in the horizontal and Charney–Phillips staggering is used in the vertical. A terrain-following vertical coordinate system is used in which the model levels follow the terrain at the surface but tend to horizontal at higher levels. A number of physical parametrizations are available in the model; these include schemes for convection (Gregory and Rowntree, 1990), two-stream radiation (Edwards and Slingo, 1996), sub-grid cloud (Smith, 1990), mixed-phase microphysics (Wilson and Ballard, 1999) with an additional prognostic variable for rain, and non-local boundary-layer mixing (Lock *et al.*, 2000). Each MetUM domain used in this study uses the Lock *et al.* (2000) boundary-layer scheme for mixing in the vertical and a two-dimensional Smagorinsky (1963) mixing scheme in the horizontal.

We make use of the MetUM as part of the Met Office Global and Regional Ensemble Prediction System (MOGREPS; Bowler *et al.*, 2008), which at the time of the case-study produced 24 different, equally likely, ensemble members (a control member and 23 perturbed members). The global ensemble had a latitude–longitude horizontal grid spacing of $0.55 \times 0.83^{\circ}$ (approximately 60 km in both directions over the UK) and 70 (non-uniformly spaced) vertical levels up to a model lid at 80 km. The initial analysis was created using 4D-Var data assimilation and perturbations around this analysis were created using an Ensemble Transform Kalman Filter; different perturbations are applied to each ensemble member except the control which is unperturbed. The model was initialised at 0000 and 1200 UTC operationally; the 0000 UTC initialisation from 27 August 2011 was used during this study (and all times given hereafter are on that date). A regional ensemble (MOGREPS-R) was created from the global ensemble. The domain for the regional ensemble was the operational North Atlantic and European (NAE) domain shown in Figure 5. Each regional ensemble member was one-way nested within the equivalent global ensemble member. The horizontal grid spacing of the regional ensemble was 18 km and it had the same 70 vertical levels as the global ensemble. The boundary conditions for the regional domain were taken directly from the global ensemble members, whereas the initial conditions for the regional ensemble members were created by perturbing the operational analysis for that domain (which included a full 4D-Var data assimilation cycle). The initial perturbations for the regional ensemble were taken from the global ensemble by computing the difference between that ensemble member and the global control member at the initialisation time for the regional ensemble. The 'random parameters' stochastic physics which are used in the operational regional ensemble were not used in this study, so creating an 'initial condition' ensemble in which all variation between ensemble members arises from their different initial conditions. A 21 (rather than 24)-member ensemble was used in this study because the boundary-condition data were unavailable for three ensemble members (members 18, 20 and 22).

A high-resolution, convection-permitting, MetUM configuration was one-way nested directly within each regional ensemble member. The regional ensemble was initialised at 0600 UTC with the high-resolution ensemble starting 3 h later. This high-resolution model was the United Kingdom Variable resolution (UKV) model; the domain is shown as the black box within Figure 5. At the time of this study, a UKV forecast was run over the UK every 6 h; it now runs operationally every 3 h. It has variable horizontal resolution; the finest grid-spacing is 1.5×1.5 km over the UK, reducing to 4×1.5 km at the edges of the domain and 4×4 km in the corners. This variable resolution allows the model to be nested within a coarser-resolution model than would be possible if the grid spacing were 1.5 km over the whole domain. The fine horizontal grid spacing of the UKV model allows it to explicitly represent convection without the need for any convection parametrization schemes. The UKV model has 70 vertical levels with a model lid at 40 km (and so higher vertical resolution than the global and regional ensemble models). Both the initial conditions and boundary conditions are taken directly from the regional ensemble members; there is no additional data assimilation and the regional ensemble members are 'downscaled' to produce initial and boundary conditions for the high-resolution ensemble members. We find that the UKV model takes around 4–6 h to spin up features on the grid scale due to the coarser-resolution initial conditions. The Met Office began routinely running a 2.2 km grid-length ensemble forecast over the UK in 2012 (MOGREPS-UK). This ensemble was not operational at the time of the case-study chosen and the decision to create a UKV model ensemble, rather than mimic the MOGREPS-UK configuration, was made because the slightly higher resolution is more suitable for the correct representation of narrow convective bands.

Results are presented from a control ensemble (hereafter CTL) in section 4. Perturbed-terrain height ensembles are presented in section 5.

4. CTL ensemble simulations

4.1. Ensemble verification

The UKV ensemble simulations are broadly in agreement with observations. The synoptic scale is well predicted and is consistent across the ensemble. The location of the surface low pressure in the North Sea and the rest of the synoptic pressure pattern are consistent with the 1200 UTC analysis shown in Figure 3, as would be expected of a short-lead-time forecast (not shown). Differences exist in the rainfall upstream of the Lake District prior to the formation of the band, with the radar showing numerous showers but the ensemble simulations producing little or no rain in this region. The lack of upstream rain is possibly a result of the model atmosphere having too little convective instability at this time. Alternatively, the lack of rain could be an indication that the 1.5 km grid spacing is insufficient to represent shallow convective showers or that that the model cannot produce showers of this small scale during the spin-up period. Unfortunately, there are no atmospheric soundings available in this region against which to compare the model.

In the region upstream of the band formation, land surface station observations extracted from the Met Office Integrated Data Archive System (MIDAS) show that the observed magnitude of the diurnal cycle of temperature is underestimated by the ensemble. The bias in the diurnal cycle is fairly consistent across all ensemble members (not shown). This results in a cold bias of 2–3°C in the maximum temperature over the Lake District prior to the initiation of the observed band. The low-level wind is also too strong in the ensemble simulations, by an average of $1.3\ \mathrm{m\,s^{-1}}$, when compared to surface stations across the Lake District in the few hours preceding the band formation. Despite these biases, some ensemble members are able to produce stationary banded rainfall of the correct intensity in the right location and at the right time; therefore, no attempt has been made to correct the model biases.

The ensemble yields a substantial spread in rainfall; in the location where the band was observed there is large variability in the amount, duration and distribution. This variability suggests that, even if the model topography is important for governing where, when and how much rain falls, it is not the sole factor. Other factors, ranging in scale from synoptic-scale pressure patterns to small-scale temperature variations, are also important.

In general, the ensemble simulations fail to produce banded rainfall in the region of the observed band, although most do produce some rainfall over this general area. In ensemble members where banded rainfall is produced in this region, it initiates too far downstream, produces too little rain compared to the radar,

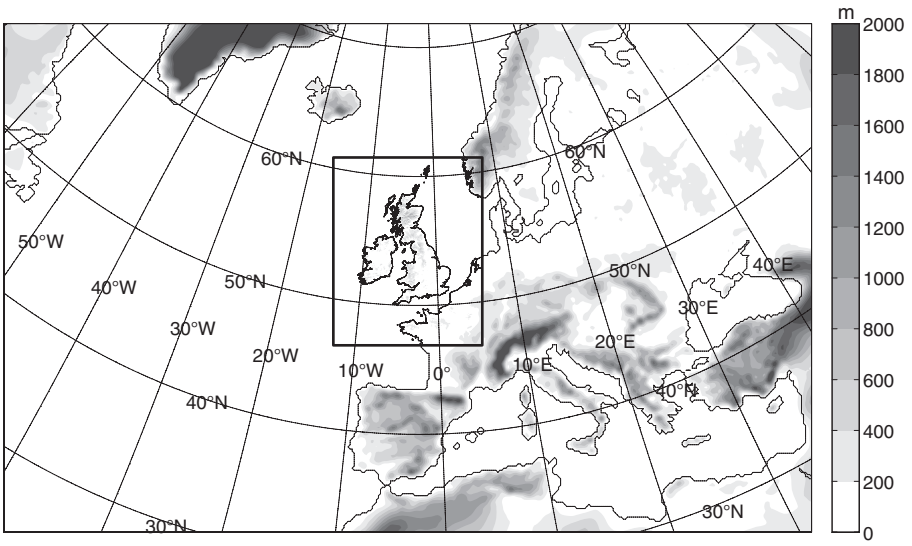

Figure 5. Model domains for MOGREPS-R simulations which use the NAE domain (whole figure) and the UKV model (inner rectangle). The shading shows the model terrain height for the respective models and the contours show the model coastlines.

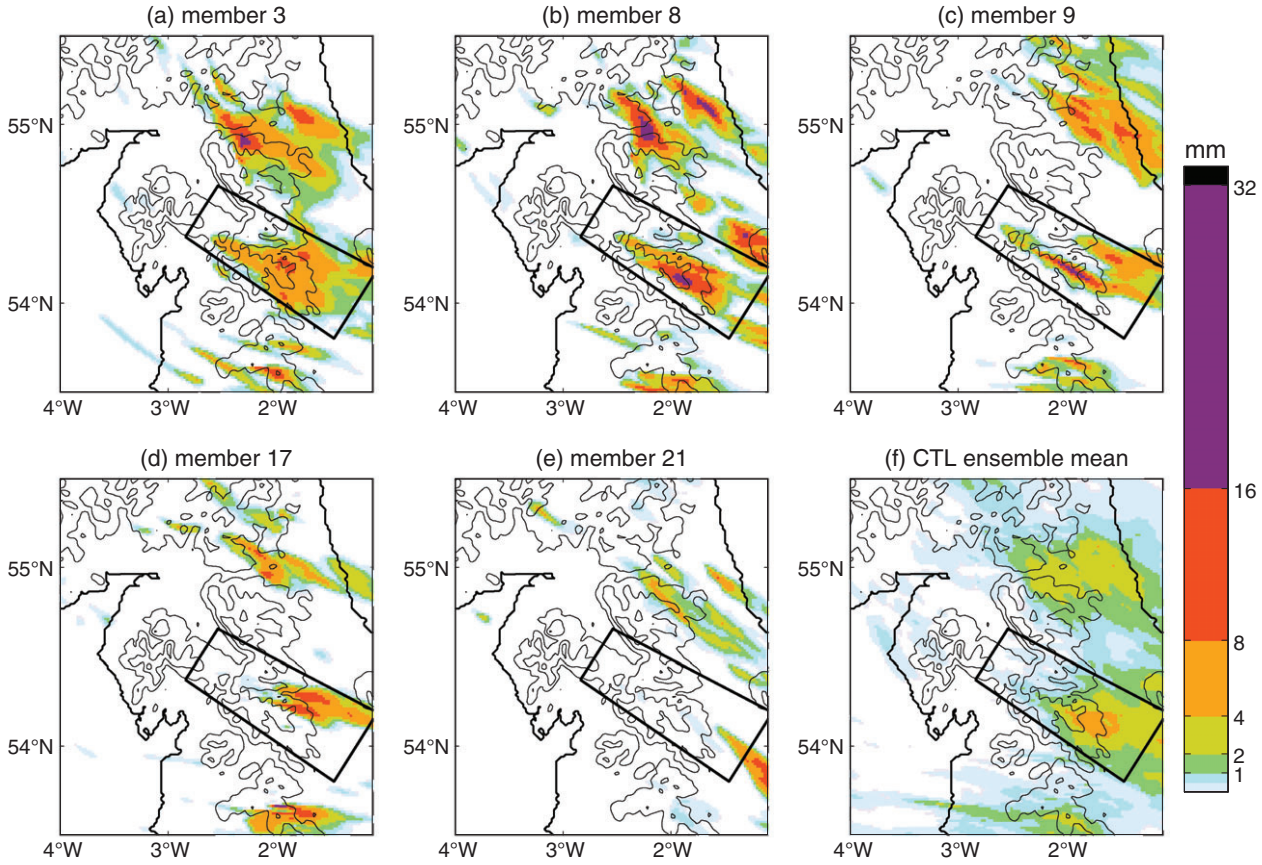

Figure 6. Three hour rainfall accumulations from 1500 to 1800 UTC from five different ensemble members from CTL and the ensemble mean. The black box on each panel defines the area over which quantitative comparisons are performed. Contours show the coastline (bold black line) and surface elevation at intervals of 200 m starting at 200 m above mean sea level (thin black lines).

and tends not to be stationary. Despite this, four of the 21 ensemble members produce some banded rainfall at, or close to, the observed band location, and this is stationary for more than 30 min in three members. In particular, member 9 stands out because it produced a linear band of rainfall accumulation in the exact location of the observed rainband with maximum accumulations of 21 mm, compared with 34 mm from the radar accumulation (Figure 6(c)). The upwind edge of the simulated rainfall structure remains anchored to the terrain for 90 min before moving downstream, exhibiting similar behaviour to the radar-derived rain, except for its shorter duration. Other ensemble members also produce banded rainfall accumulations (e.g. member 8; Figure 6(b)), but many of these accumulations derive from convective cells moving along the band axis rather than stationary rainfall. In contrast, some ensemble members have rainfall accumulation patterns that are quite different from those observed. For example, member 7 has a wind field that is too zonal compared to observations and hence produces almost east–west oriented rainfall accumulations (not shown). In another example, member 3 produces rainfall at the observed location and also produces much higher rainfall accumulations farther north (Figure 6(a)) than those observed. The ensemble mean rainfall accumulation (Figure 6(f)) shows the ensemble generally producing rainfall in the correct location, but the accumulations are lower and spread over a larger area than observed, as would be expected from the mean of 21 ensemble members.

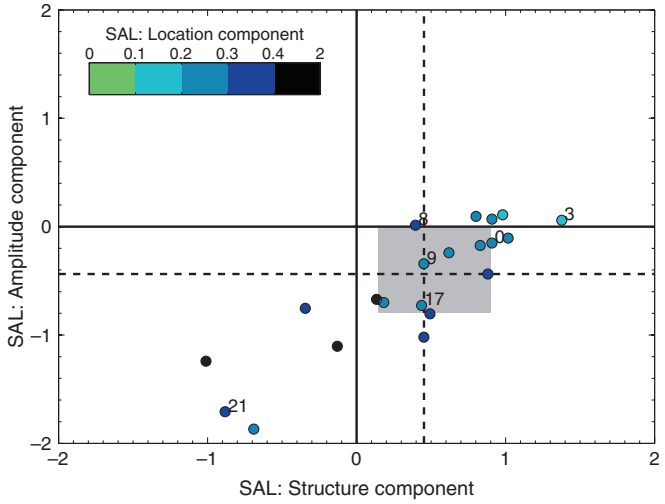

Figure 7. SAL diagram showing the structure, amplitude and location errors of the rainfall in the individual ensemble members in CTL. A perfect prediction would have values of 0 for each component. The dashed line shows the median values of S and A, whilst the grey box spans their 25th to 75th percentiles. Selected ensemble members (those shown in Figure 6 and the control member) are labelled.

4.2. *Object-based rainfall verification*

We use an object-based rainfall verification method to quantify the skill of the model, avoiding the 'double-penalty' problem associated with grid-point-based skill scores. This method, known as SAL (Structure, Amplitude and Location) and developed by Wernli *et al.* (2008), is briefly described below.

4.2.1. *Method*

The SAL method objectively determines the characteristics of the rainfall field from both forecasts and observations and scores the forecast by comparing these characteristics. The three characteristics measure the differences in structure (S), amplitude (A) and location (L) of the rainfall accumulation fields. Before doing this comparison, the radar data (1 km grid) was reprojected on to the model grid (1.5 km) by selecting the nearest radar pixel to the centre of the model grid box. This reprojection makes little change to the characteristics of the radar rainfall field.

The amplitude component considers the domain-average rainfall. Both the structure and location components compare the statistics of the individual rainfall objects in the model and observation rainfall fields. The structure component compares the proportion of high and low rainfall totals within each object. The location component quantifies the physical distance between the centres of mass of the two rainfall fields. Values for the amplitude and structure components are in the range $[-2,\ 2]$, where 0 denotes a perfect forecast of rain amount and ± 0.66 represents a factor of two error. The location component ranges from 0 to 2, where zero is a perfect forecast with larger values indicating a greater separation between centre of mass of the two rainfall fields.

The structure and location components both require individual rainfall objects to be identified. This is done by selecting a threshold value of 1/15 of the maximum rainfall accumulation in the domain (chosen following Wernli *et al.*, 2008). The structure and location components are thus independent of the total rainfall in the domain, which is measured by the amplitude component.

4.2.2. *Results*

The performance of the ensemble is summarised using the SAL diagram (Figure 7). The rainfall fields compared are the 3 h accumulations, from 1500 to 1800 UTC, over the region of observed banded rainfall, as marked in Figure 6. A large spread of values for both amplitude and structure components are observed. The amplitude component is below zero for 16 of the 21 ensemble members, implying underprediction of the total rainfall in this region by the majority of the ensemble. A value of -0.66 represents ensemble members producing only half of the observed rainfall, and almost half of the ensemble members perform at least this poorly. Sixteen of the ensemble members have a positive value for the structure component, with a median value of 0.45, implying forecast rainfall objects are too large or too uniform (i.e. lacking peak accumulation values). This error is expected given the 1.5 km grid spacing of the model and the relatively narrow width of the observed band. There is also a strong positive correlation between the structure and amplitude components, showing that larger area-averaged rain accumulations are produced by larger, more uniform rainfall objects. There is much less variability in the location component, with 16 of the 21 ensemble members having values between 0.2 and 0.4.

In summary, some ensemble members forecast weak stationary banded rainfall in the location of the observed band. The rainfall accumulations in these simulations are less than observed but still substantial for a 3 h period. Other ensemble members forecast similar rainfall accumulations nearby but fail to represent either the banded structure or the stationarity, and often lack both. Some poorer members do not produce any similar feature. This spread in forecast skill suggests that the formation of the band is highly sensitive to the initial conditions.

4.3. *Ensemble sensitivity analysis*

Ensemble sensitivity analysis (Ancell and Hakim, 2007; Torn and Hakim, 2008) is used to quantify the sensitivity of the precipitation band to uncertainties in the larger-scale flow field. It quantifies how selected model fields are related to a particular aspect of the forecast outcome. Specifically, the environmental properties associated with persistent rainfall in the location near the observed band were assessed; the duration of this rainfall is here referred to as the 'response function'. This method allows spatial relationships between the environmental properties and the response function to be understood. However, as this method is based on linear regression and correlation coefficients, it cannot establish causality.

4.3.1. *Method*

Here we assess the association between a particular test variable, such as surface pressure, and the response function using data from the whole set of ensemble members. The ensemble sensitivity S is defined as

$$S = m\, a\, \sigma_x ,$$

where the regression coefficient m between the test variable (x) and the response function (y), which is calculated at each grid point, provides a raw measure of the sensitivity. The scaling factor a is used to de-emphasise noise when the correlation between x and y is weak, as quantified by their correlation coefficient r: when $r^2 \geq 0.1$, $a = 1$ and when $r^2 < 0.1$, $a = r^2/0.1$. Multiplication of $m\,a$ by the ensemble standard deviation of the test variable (σ_x) at each grid point yields a two-dimensional sensitivity field with units matching those of the response function. This scaling allows the sensitivity of the response function to be quantitatively compared for different test variables.

4.3.2. *Results*

In the forthcoming analysis, the response function is defined as the maximum duration of continuous rain (greater than 1 mm h^{-1}) at any grid point within the observed band region, as marked in Figure 6. This metric was chosen instead of the total rainfall accumulation within the region to better detect long-lasting stationary rainfall. However, the two methods produce

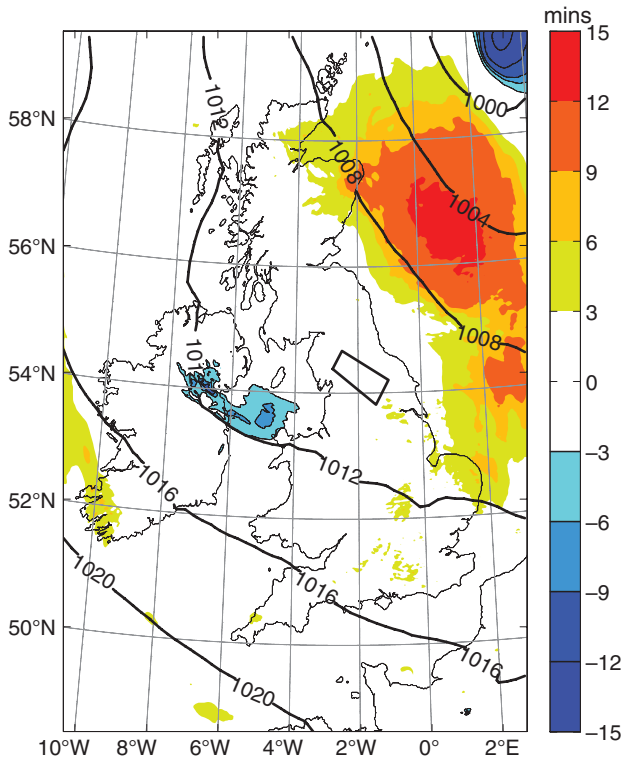

Figure 8. Map of the sensitivity of rainfall duration to changes in surface pressure at 1200 UTC 27 August, calculated using ensemble sensitivity analysis. The values plotted represent the change in rainfall duration of the band for a one standard deviation increase in the pressure at the grid point plotted. The bold black contours show mean sea level pressure (hPa) for the control ensemble member at 1200 UTC. Negative sensitivity values are contoured with a thin black line. The black box from Figure 6 is also marked.

qualitatively similar results, indicating that the highest rainfall accumulations do indeed come from the more stationary rainfall features.

Figure 8 shows the ensemble sensitivity of rainfall duration to surface pressure at 1200 UTC 27 August. A strong association is found between enhanced rain duration and higher pressure in the North Sea (centred at 1°E, 57°N) to the southwest of the surface low pressure centre and lower pressure to the east and northeast of the low centre (in the top right corner of the figure). The rainfall duration increases 12–15 min for each standard deviation increase in pressure in the North Sea. This pressure sensitivity pattern can be interpreted as a preference for longer-duration rainfall when the low centre is shifted towards the east or northeast. Additionally, a weaker association with lower pressure is seen in the Irish Sea (near 5°W, 53.5°N), which, together with the association with high pressure in the North Sea, implies longer-duration rainfall when there is a weaker pressure gradient across the British Isles and consequently weaker geostrophic winds upstream of the Lake District. Evidently, relatively small variations in the synoptic and mesoscale forcing of the event can produce significant variations in the duration of the banded rainfall.

The six panels of Figure 9 show ensemble sensitivity analysis results for other variables (performed over a smaller domain). Except for CAPE, the values used are from the fifth model level (111 m above ground level) but the conclusions were insensitive to the model level chosen, provided the model level was within the boundary layer (not shown). CAPE was calculated using the most unstable lifted parcel from the lowest 433 m above ground level with the value representing the area of positive buoyancy in the sounding only. The sensitivities are calculated using model variables from 1400 UTC, approximately 1 h before the band forms. Figure 9(a, b, c) show an association of longer-duration rainfall with lower temperature and reduced humidity upstream (to the northwest) and over the Lake District. There is also an association with lower CAPE values northwest of the Lake District, indicating that longer-duration rainfall is associated with more stable upstream flow. In contrast to the Castor Bay sounding (Figure 4), the simulated flow closer to the band does possess significant moist instability. Ensemble-mean CAPE (306 J kg^{-1}) and convective inhibition (CIN; 12 J kg^{-1}) just upstream of the Lake District suggest an environment supportive for cumulus convection. Evidently, this instability was released primarily within the convective band downwind of the Lake District. This presence of longer-duration rainfall when CAPE is lower should be interpreted within the range of ensemble values. Clearly, instability is required for the band to exist, but ensemble members with larger CAPE values in the upstream flow release the convective instability over the Lake District itself or in other locations, rather than requiring the extra forcing from lee-side convergence to release the instability. The association of longer-duration rainfall with lower temperatures over the region in which the band forms is due to a pre-existing cloud band over this area at 1400 UTC in simulations that eventually produce a long-duration rainfall event. Figure 9(d, e, f) show an association of longer-duration rainfall with weaker winds over the whole domain (Figure 9(d)) especially the zonal component of the wind speed (Figure 9(e)), which is consistent with the association for a weaker pressure gradient upstream of this area (Figure 8). The sensitivity to meridional wind (Figure 9(f)) shows that longer-duration rainfall occurs when there is more northerly flow to the north and more southerly flow to the south of the band location (i.e. increased convergence in the lee of the Lake District where the band forms).

4.4. *Froude number analysis*

The ensemble sensitivity analysis results are consistent with the formation of this stationary convective rainband being caused by flow separation upstream of the Lake District, resulting in flow around the elevated terrain rather than over it, and convergence in the lee where the convective band is initiated. To first order, this behaviour can be interpreted using the Froude number *Fr* (Eq. 1), where a reduction of the Froude number is associated with air that is more likely to be deflected around an obstacle rather than to flow over it. Lower values of the Froude number are associated with stronger low-level dry stability and/or slower flow approaching the Lake District. Consistent with this, there was an association between longer-duration rainfall and both weaker moist instability (Figure 9(c)) and slower flow (Figure 9(d, e, f)) upstream of the band formation region. Although the utility of *Fr*, as expressed by Eq. (1), may be reduced in situations where moist convection is released directly over the mountain barrier (e.g. Miglietta and Rotunno, 2009), here the majority of the convective precipitation occurs downwind of the Lake District (Figure 2), likely because of insufficient lifting over the barrier and gradual downwind destabilization due to diurnal surface heat fluxes over land. Because the flow directly over the high terrain was largely free of cumulus convection, Eq. (1) indeed provides a useful characterization of the orographic flow regime.

The Froude number was calculated from the ensemble of MetUM simulations, using values upstream of the Lake District and below 845 m height (lowest 15 model levels). This height is equivalent to the highest Lake District peak in the model. The wind speed, U, was calculated as the mass-weighted wind speed below this height and N^2 was calculated as

$$N^2 = \frac{g}{\theta_{15}} \frac{\theta_{15} - \theta_5}{h},$$

where $g = 9.81\ \mathrm{m\,s^{-2}}$ and θ_n is the virtual potential temperature at model level n. This bulk approach for the Froude number calculation follows Reinecke and Durran (2008), who suggested that this method was most appropriate for predicting low-level flow diversion. The Froude number for each ensemble member was calculated as an average over 451 grid points just upstream

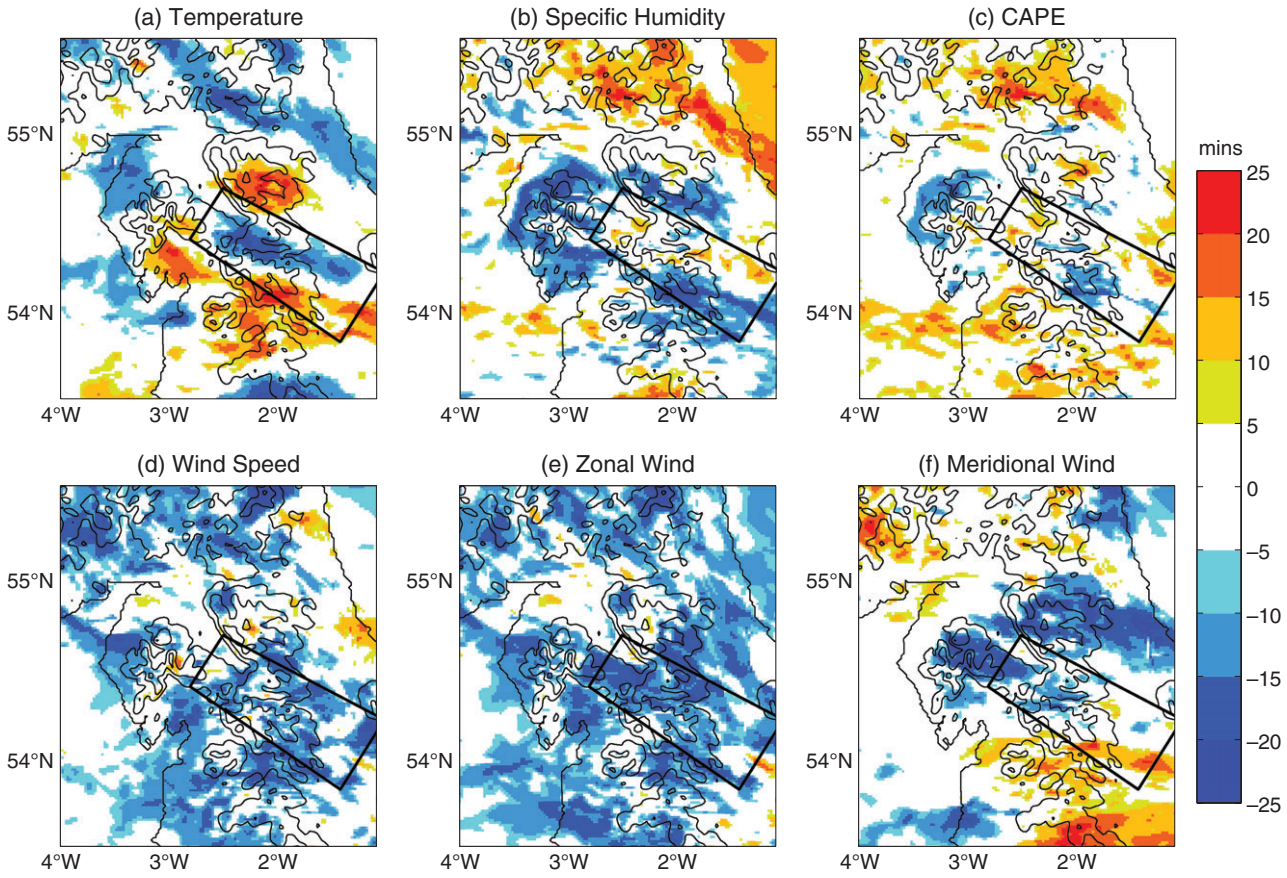

Figure 9. Maps of the sensitivity of rainfall duration to changes in (a) temperature, (b) specific humidity, (c) CAPE, (d) wind speed, (e) zonal wind component and (f) meridional wind component (all except CAPE on model level 5 (111 m above ground level)) at 1400 UTC calculated using ensemble sensitivity analysis. The values plotted represent the change in rainfall duration of the band for a one standard deviation increase of the variable at the grid point plotted. The contours show the coastline and the surface elevation with a contour interval of 200 m. The black box from Figure 6 is also marked.

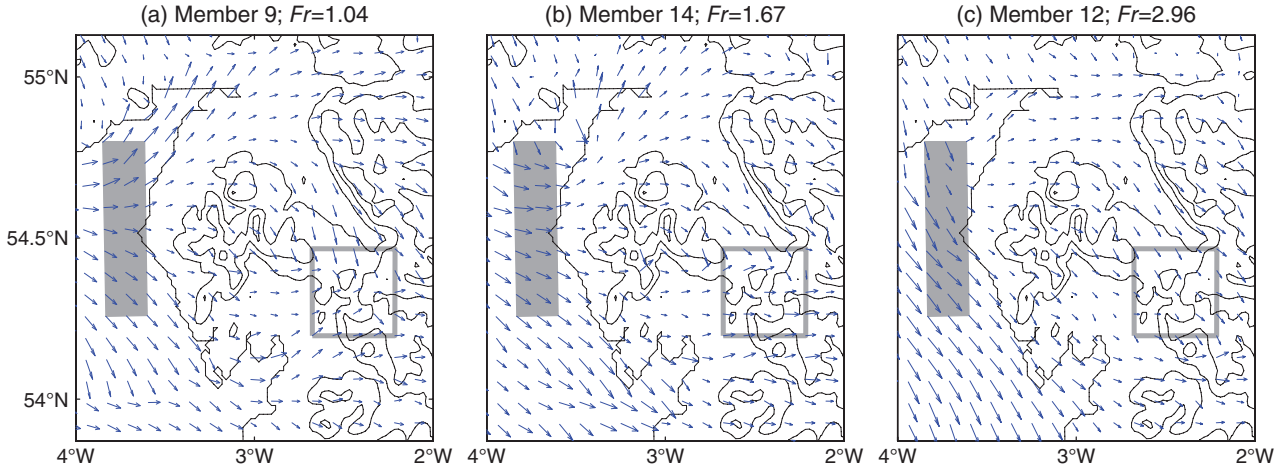

Figure 10. Wind vectors at the lowest model level (5 m above ground level) at 1400 UTC from three ensemble members: (a) member 9, (b) member 14 and (c) member 12. The wind vectors show the flow deflection around the Lake District across a range of Froude numbers. Contours show the coastline and surface elevation at 200 m intervals. The grey shaded box marks the area over which Froude numbers were calculated. The grey outlined box marks the area over which the lee-side convergence was calculated.

of the Lake District, as marked in Figure 10. The sensitivity of the calculation to the choice of area was assessed and found to make small quantitative differences (up to 0.2 for larger Froude numbers) but the relative values of ensemble members were robust across all locations upstream of the Lake District.

The lowest mean Froude number of any ensemble member was 1.02 ± 0.01 (95% confidence interval) and the largest was 2.96 ± 0.26. The Froude number is thus larger than unity for all ensemble members, suggesting air tends to flow over the obstacle rather than detour around it. This contradicts the ensemble sensitivity analysis results which show enhanced duration rainfall with enhanced flow convergence in the lee of the Lake District. However, the static stability and wind speed are non-uniform in the vertical, and consequently the calculations of the Froude number can be quite sensitive to the layer over which it is calculated (Reinecke and Durran, 2008). For example, the wind speed near the surface is reduced by friction, so the low-level air effectively has a lower Froude number and is more likely to detour around the terrain. Additionally, the model simulations show that the static stability of the boundary layer upstream of the Lake District is near zero in this case, with a sharp inversion at the top of the layer and a statically stable layer above (not shown). Any bulk or integrated measure of the static stability over the layer will thus be sensitive to the depth of layer chosen. Vosper *et al.* (2009) suggest increasing the depth of the layer over which the static stability is calculated when a jump in static stability is found near

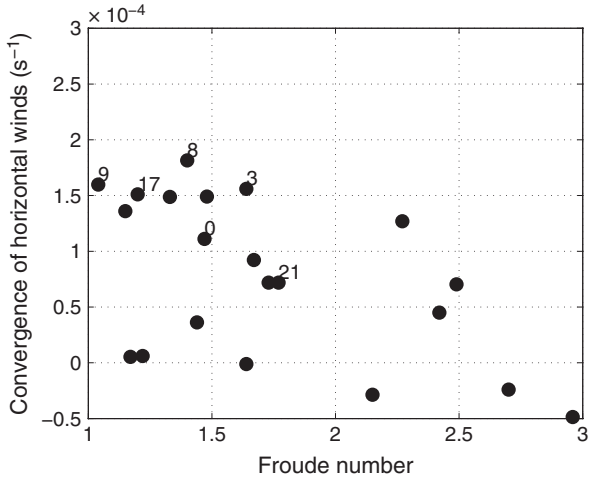

Figure 11. Scatter plot of Froude number versus the strength of the lee-side convergence, for members of the CTL ensemble. Convergence is calculated within the grey outlined box in the lee of the Lake District as marked in Figure 10. The ensemble members shown in Figure 6 are marked, together with the unperturbed control member 0.

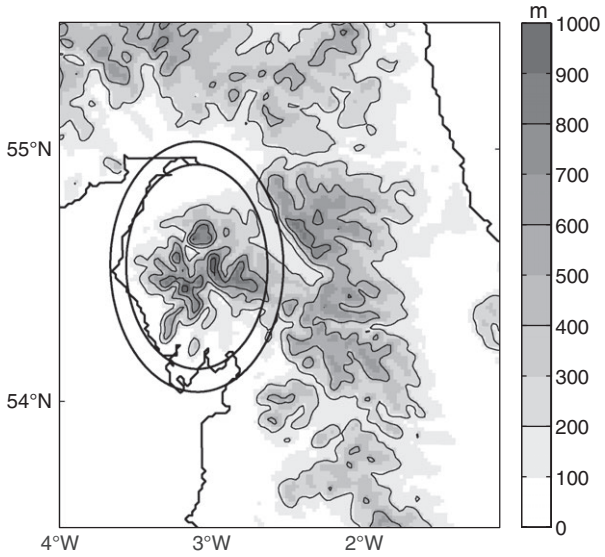

Figure 12. Model terrain height for the HIGH terrain experiments. The terrain height within the inner circle has been increased by 30% from the standard model topography. Terrain height outside the outer circle has not been changed, and the percentage increase varies linearly from 0 to 30 between the outer and inner circles. The same area of terrain was flattened in the ZERO terrain experiment, again with a linear transition between the inner and outer circles.

the peak height of the terrain. Our calculated Froude numbers are reduced by an average of 15% when calculated following Vosper *et al.* (2009), resulting in two ensemble members with values below unity. There is evidence for flow blocking and deflection around the Lake District in the ensemble members with the lower Froude numbers, despite the absolute value being larger than unity (Figure 10); the amount of deflection reduces as the Froude number increases. Therefore, the spread of Froude numbers calculated across the ensemble is indicative of variability in the degree of flow blocking in the ensemble members, with the flow in some members being partially blocked, despite possessing $Fr > 1$. This point is illustrated by Figure 11, where the strength of convergence on the lee side of the Lake District increases with decreasing Froude number, even though all values of Fr are greater than unity. There is clearly evidence for flow separation around the Lake District and lee convergence in ensemble members with more flow deflection occurring when Fr is lower.

5. Perturbed terrain height ensemble simulations

The control ensemble (described in section 4) highlighted that the existence of the rainband required particular upstream flow conditions (i.e. weak winds) such that terrain organised the flow to produce convergence in the lee. To demonstrate the importance of the terrain in the formation of this band, further ensemble experiments were performed where the terrain height was modified. The terrain of the Lake District and the Yorkshire Dales were modified independently, but only simulations where the Lake District terrain was modified are described because the role of the Yorkshire Dales in organising the rainfall was relatively minor. Two experiments were performed, the first experiment (ZERO) had the Lake District terrain height reduced to mean sea level whereas the second experiment (HIGH) increased the terrain height of the Lake District by 30%. In both experiments the land-surface properties were not changed. The changes to terrain height were applied inside the inner circle marked in Figure 12. The terrain height between the inner and outer circle was also modified to ensure a smooth transition to the default topography, achieved by linearly relaxing the terrain height back to the default values between the inner and outer circles.

5.1. *ZERO experiment*

Removing the Lake District terrain from the ensemble members affects both the location and amount of rainfall downwind of the terrain changes. The changes described are for CTL minus ZERO, and therefore express the impact of the terrain in CTL relative to simulations without it. There is a substantial increase in the rain accumulation along the axis of the observed band resulting from flow interactions with the terrain, but a reduction in rainfall to both sides (Figure 13(a)). The rainfall is less organised in the ZERO simulations and therefore, the rain falls over a larger area with lower accumulations than in CTL. In fact, the individual cells are also less organised (not shown) with none of the ensemble members producing any banded or stationary convective features without the presence of the Lake District. The overall rainfall (1500–1800 UTC) within the banded area increases by 33% when the Lake District is present, which is an increase of the area-averaged rain rate of 1.25 mm h^{-1}.

With the Lake District terrain present, the flow is deflected around the upstream terrain resulting in slower winds upstream and downstream of the Lake District, but faster winds over the crest of the Lake District and in the valley to the northeast (Figure 13(e, f)). In addition, the flow approaching the Yorkshire Dales is both warmer (Figure 13(b)) and drier (Figure 13(c)) on average in CTL than in ZERO. These effects, which arise in part from downwind mountain-wake formation and adiabatic warming, both act to decrease the relative humidity of the boundary layer and raise the lifting condensation level, making cloud (and rain) formation on the upslopes of the Yorkshire Dales less likely. The relative humidity changes are consistent with a broad decrease of the mean cloud liquid water path (vertical integral of cloud liquid water content; Figure 13(d)). Notably, the liquid water path increases along the axis of the band, consistent with that of the rainfall distribution (Figure 13(a)). There is also an increase in cloud amount at the upwind edge of the Lake District (Figure 13(d)).

Both the cloud and rain distribution are more focused along the band axis in CTL than in ZERO. This pattern of changed cloud and rain amounts results from the lower relative humidity over a large area but increased convergence along the axis of the band (Figure 13(f)). Therefore, the presence of the Lake District contributes to the existence of the band by focusing lee-side convergence and vertical motion downwind of the Lake District.

5.2. *HIGH experiment*

The changes between the HIGH and CTL ensembles are similar to the changes between CTL and ZERO although smaller as the absolute change in terrain height is smaller. More rainfall is

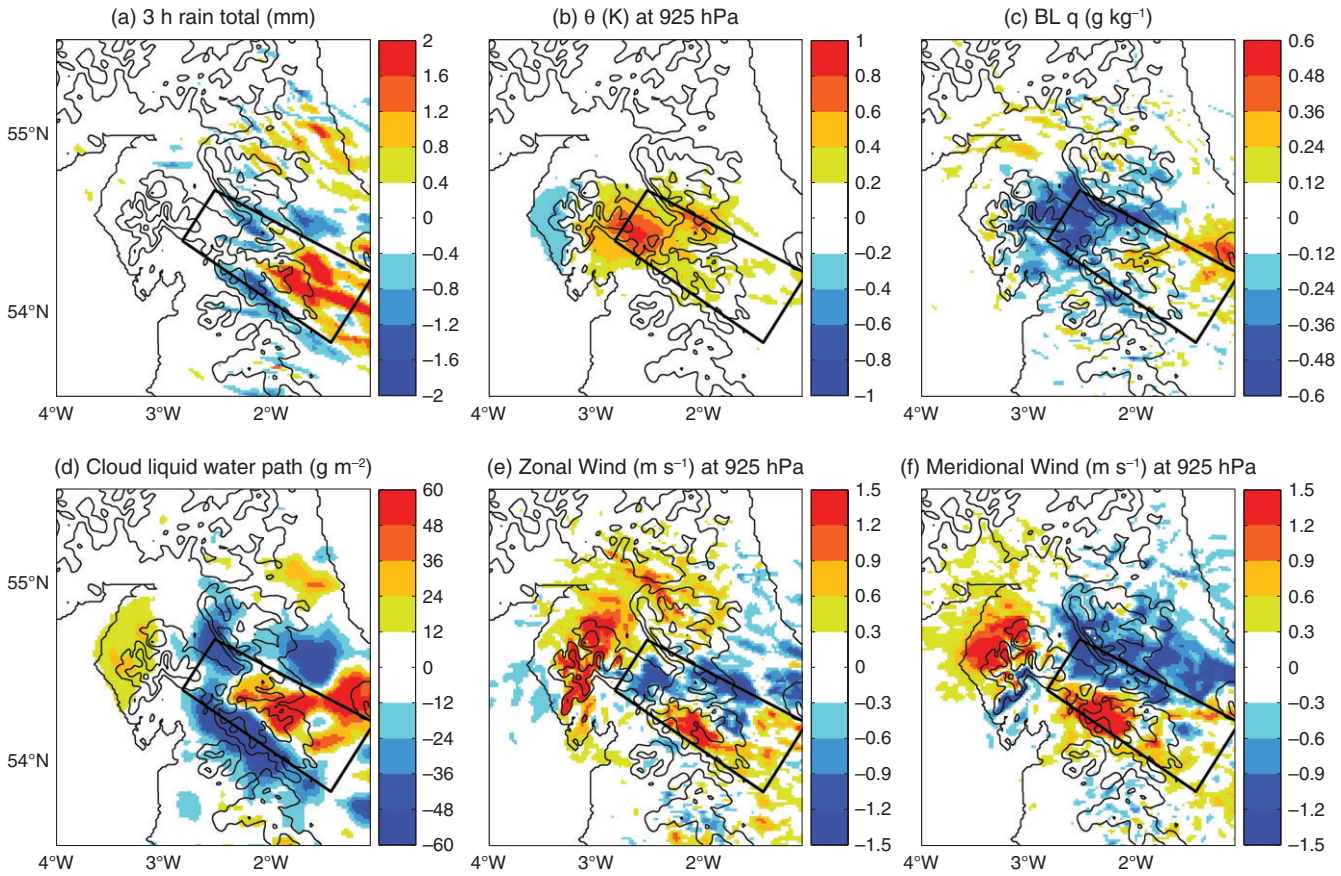

Figure 13. Differences between the ensemble means of ZERO and CTL (CTL minus ZERO; at 1400 UTC unless stated otherwise) showing the effect of the Lake District terrain on the simulations: (a) rain accumulation from 1500 to 1800 UTC, (b) potential temperature at 925 hPa, (c) boundary-layer specific humidity at 111 m above ground level, (d) cloud liquid water path (with a 2D smoothing to de-emphasise noise), (e) zonal and (f) meridional wind speed at 925 hPa. The contours show the coastline and the surface elevation for CTL with a contour interval of 200 m. The black box from Figure 6 is also marked.

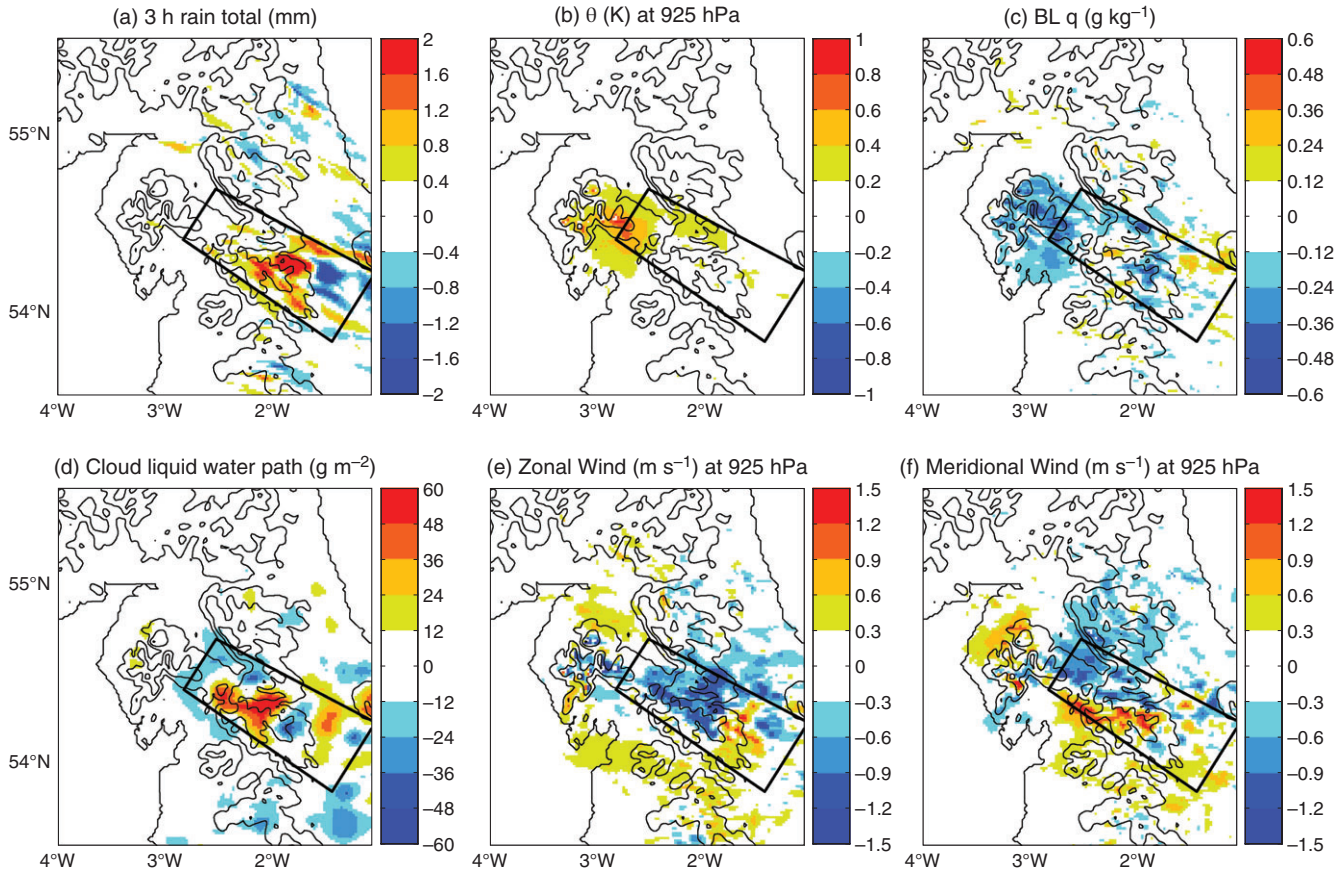

Figure 14. As Figure 13, but showing the differences between the HIGH and CTL ensemble (HIGH minus CTL).

produced downstream of the Lake District in the HIGH ensemble, and the rainfall also moves nearer to the Lake District, in better agreement with radar observations. The rainfall accumulations increase by 1–2 mm along the band axis (Figure 14(a)) with a reduction in the rainfall accumulations farther downstream. The banded-area 3 h total rainfall increases by 17% and is stationary for 25 min longer. The location of maximum rainfall accumulation moves 20 km upstream in HIGH relative to CTL.

Increasing the terrain height resulted in slightly weaker winds over the crest of Lake District, but stronger winds on the southern flank and in the valley to the northeast (Figure 14(e, f)). This enhanced deflection of the flow around the Lake District is consistent with the reduced Froude number associated with the raised terrain height. The boundary layer over and downstream of the Lake District was warmer and drier in HIGH than in CTL (Figure 14(b, c)). Again, the mean liquid water path increases over and downstream of the point where the observed band initiates (Figure 14(d)), whereas it decreases in surrounding areas; the same areas also experience an increase in the rain accumulation (Figure 14(a)). These changes are again due to a drier boundary layer (Figure 14(c)) and enhanced lee-side convergence (Figure 14(f)) caused by the higher terrain.

The higher boundary-layer potential temperatures over the Lake District in HIGH relative to CTL (and in CTL relative to ZERO) are due to stronger elevated heating over the higher terrain, where the physically higher terrain surface acts as a localised heat source. The higher the terrain surface, the stronger the effect of the heating becomes relative to surrounding air. This change in temperature over the elevated terrain has the largest magnitude on the downwind side of the terrain (Figures 13(b) and 14(b)) as the heat is continually advected past the Lake District. This elevated heating may be important in initiating or enhancing a convergent circulation in the lee of the terrain.

Figure 15 shows the SAL metrics for HIGH and is directly comparable to Figure 7 for CTL. The number of outliers in the ensemble has been reduced in HIGH (e.g. only one member with structure component below −0.5 compared with three in CTL), the inter-quartile range (grey box) has reduced for both structure and amplitude components, and the mean (not shown) and median (dashed line) have moved towards zero. This increase in ensemble skill for this ensemble with reduced Froude number is consistent with the finding that most skilful members in CTL had the lowest Froude number (where here lower Froude number was associated with weaker upstream wind speeds and stronger upstream stability). In addition, the mean location error of the ensemble has reduced.

The increased Lake District terrain height, and effectively lower Froude number in this ensemble, favours stronger upstream blocking. As a consequence, the flow converges more strongly in the lee of the Lake District, giving rise to stronger and more persistent downwind convection bands. Hence, by compensating for a systematic overprediction of upstream wind speed (and correspondingly high Froude numbers) in the CTL ensemble, the HIGH ensemble provides a more accurate representation of the orographic flow regime and, in turn, a more accurate forecast.

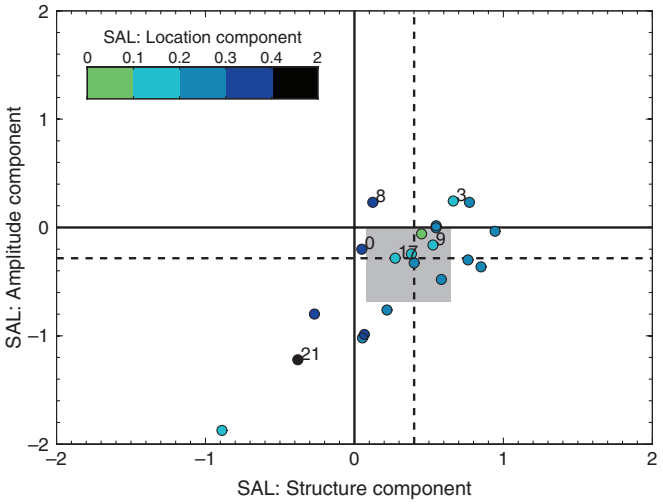

Figure 15. SAL diagram showing the structure, amplitude and location errors of the rainfall in the individual ensemble members in HIGH. This should be compared with Figure 7 which shows the same metrics for CTL.

6. Attribution of convergence to thermal and mechanical forcing

There are two possible mechanisms through which increasing the height of the terrain may affect the rainfall: (i) the air is more likely to flow around (rather than over) a higher obstacle and (ii) the heated surface of the Lake District acts as a stronger heat source because it is surrounded by cooler air. This differential heating generates a thermally direct circulation with the warm air rising in a band extending downwind of the terrain, surrounded by cooled descending air (e.g. Crook and Tucker, 2005).

Two simulations were run to isolate the effects of elevated heating and mechanical deflection. These simulations use the best performing member from HIGH and CTL (member 9). In both simulations, the elevated heating was removed by changing the surface albedo over the Lake District to 1, and hence reflecting all incident solar radiation (ALB1). Changing the albedo prevents the Lake District terrain from warming and acting as a heat source to the atmosphere. This change was applied to simulations using the terrain from CTL (simulation CTL+ALB1) and the terrain from HIGH (simulation HIGH+ALB1). By comparing these simulations with member 9 from HIGH, the relative importance of the mechanical and thermal effects can be determined.

The mechanical forcing (derived from HIGH+ALB1 minus CTL+ALB1) and the thermal forcing (derived from HIGH minus HIGH+ALB1) of the terrain on the meridional component of the wind are shown in Figure 16. The response to both the mechanical and thermal forcing are similar in sign, magnitude and location. This similarity indicates that both forcings are important in producing the lee-side convergence and thus the rainband. The change resulting from the mechanical forcing, where the flow is more strongly deflected around a higher obstacle and converges in the lee, is a narrow line of strong convergence focused along the axis of the simulated band. The thermal forcing has a similar convergent flow response; however, the convergence is not as narrowly focused. In the latter, the changes to the wind field are wider-ranging, affecting locations farther to the north and south as well as having a stronger influence on the slopes of the Lake District itself. Therefore, when the terrain is raised, mechanical and thermal forcings act in phase to strengthen the convergence downwind of the Lake District.

Reducing the amount of elevated heating over the Lake District reduced the amount of rainfall in the banded region, but not in other regions nearby (not shown). This suggests that there is a strong influence of the surface heating on the organisation and distribution of the rainfall. The poorly simulated diurnal cycle of temperature over the Lake District (section 4.1) could have a sizable impact on the flow given that the bias (2–3 °C) is a few times larger than the change in temperature in the simulation with changed albedo (about 0.7 °C).

The strength of the mechanical deflection and the elevated heating are both controlled by the Froude number. Stronger deflection of the flow around the Lake District was seen in CTL for members with weaker upstream winds and therefore lower Froude number. Similarly, the deflection of the winds increased when the terrain height was increased in the HIGH simulation (not shown). Additionally, increased elevated heating occurs in CTL for members with a lower Froude number (Figure 17, showing the change in near-surface temperature for a one standard deviation increase in upstream Froude number). Therefore, the two forcing mechanisms work together in this case – enhanced mechanical deflection and elevated heating are both associated with a lower

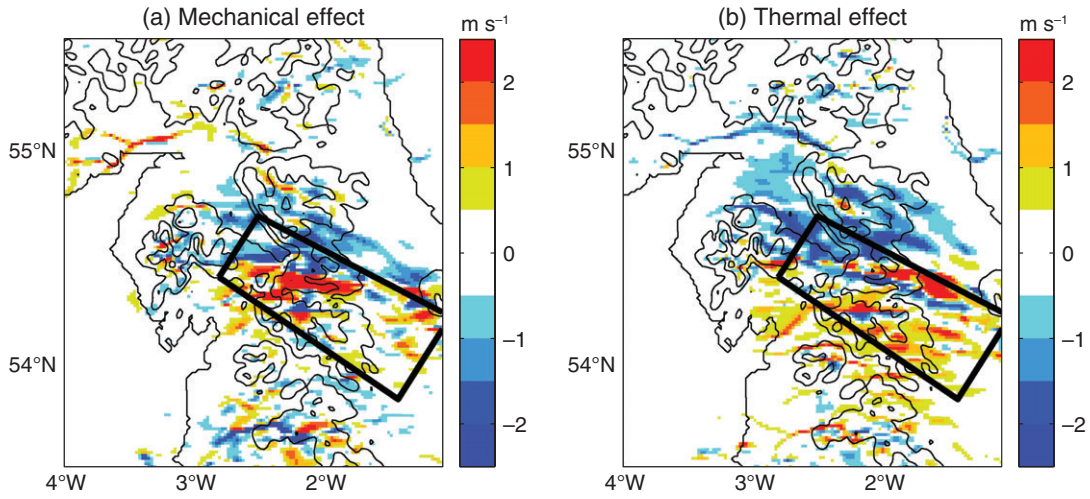

Figure 16. Difference of the meridional component of the wind at 1400 UTC between the member 9 simulations. (a) HIGH+ALB1 minus CTL+ALB1, which shows the impact of increasing the Lake District terrain height by 30% while keeping the surface albedo at 1 in both simulations. (b) HIGH minus HIGH+ALB1 which shows the impact of elevated heating when using the default albedo with the terrain height constant. The black contours show coastline and the CTL terrain height contoured every 200 m. The black box from Figure 6 is also marked.

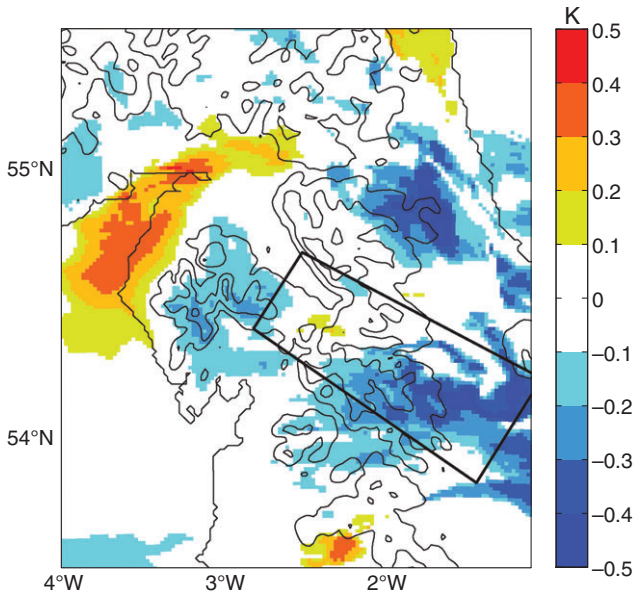

Figure 17. The temperature (at 111 m above ground level) response to a one standard deviation increase in the Froude number in CTL at 1400 UTC. Values are calculated using ensemble sensitivity analysis. The black box from Figure 6 is also marked.

Froude number and both act to cause stronger convergence in the lee of the Lake District.

7. Conclusions

High-resolution ensemble simulations of an observed orographically induced stationary convective rainband reveal that an in-phase response of mechanical and thermal forcing is responsible for the persistence of the band. The mechanical forcing results in convergence in the lee of the Lake District due to deflection around the upstream terrain. This convergence occurs because it is energetically easier for the air to flow around the obstacle rather than over it due to weak winds and a statically stable atmosphere. (Theoretically, this flow deflection requires a Froude number less than unity but estimated values are close to or slightly greater than unity here.) In addition, an area of elevated heating over the Lake District leads to convergence downstream. Elevated heating of air over the Lake District produces warmer, more buoyant air downstream and in turn results in ascent in this region and horizontal convergence at low levels. The resultant circulations from these two mechanisms superimpose to repeatedly initiate convection in the location of the rainband.

The mechanisms involved in the formation of this band are captured by the 1.5 km grid-spacing model. Despite the model performance in some ensemble members, a realistic stationary band was present in only three of the 21 members in the control ensemble. The lack of predictability appears to stem primarily from a bias toward overly strong upstream winds and, consequently, an overly high Froude number. The amount of elevated heating over the Lake District is also important; the simulations suggest that changes of a few tenths of a degree are enough to alter the simulated rainfall. Hence, accurate predictions of the pre-existing cloud cover and surface conditions are needed to simulate the rainfall accurately. Within the ensemble, small perturbations in a number of different aspects of the model (upstream wind speed, upstream stability, and the amount of elevated heating over the Lake District) result in a large spread of simulated rainfall. Such large variability in the prediction of small scales, resulting from subtle changes in the large-scale flow, demonstrates the value of and need for ensembles for convective-scale, short-range forecasting.

Increasing the height of the Lake District in the ensemble simulations led to the rainband becoming more accurate and consistent between ensemble members. The total rainfall increased and the centre of the rainfall moved upstream and nearer the terrain that caused the band, in better agreement with the observations. The skill of the individual ensemble members improved and the spread amongst them reduced, suggesting a more robust band under stronger terrain forcing. This improved skill likely results from an improved representation of the orographic flow regime. The higher terrain decreases the Froude number and hence the flow is deflected around the terrain in more of the ensemble members. The increased terrain height thus tends to offset the overly strong wind speed bias in CTL (by reducing the Froude number) and shifts the flow regime toward the upstream-deflection/lee-convergence that results in the band formation. The presence of the Lake District is vital in setting the right flow conditions to enable repeated convection initiation on the upslopes of the Yorkshire Dales.

This study has highlighted a major challenge facing convective-scale ensemble numerical weather prediction: the importance of correct representation of both small-scale structures and large-scale uncertainty. The small-scale structures include the local terrain, and temperature, humidity and wind fields which are crucial in locating when and where these convective storms occur. The model requires high resolution to capture these structures. On the other hand, the forecast can be sensitive to even small changes of the synoptic-scale flow, especially if this leads to a

change in its interaction with the terrain. Successful prediction of such high-impact events therefore requires an ensemble of models that have high resolution so as to capture the small-scale interactions and sample the uncertainty controlled by the large scale. Unfortunately, running ensembles of convective-scale models is computationally expensive, limiting the number of ensemble members. However, as this study demonstrates, a single deterministic convective-scale model simulation (i.e. an individual ensemble member) may only have a small probability of successfully predicting these quasi-stationary rainfall events and, even if it were to do so, would give no indication as to the likelihood of it actually occurring.

Acknowledgements

This work has been funded through the Natural Environment Research Council (NERC) as part of the PRESTO (PREcipitation STructures over Orography) project (NE/1024984/1). We would like to thank the Met Office for making the MetUM available for research purposes and to the National Centre for Atmospheric Science (NCAS) Computational Modelling Support (CMS) for providing technical support, in particular via Willie McGinty. We would also like to thank Humphrey Lean, Simon Vosper, Paul Field and Stuart Webster for useful discussions. We also thank two anonymous reviewers for their comments, which helped improve this manuscript. Research data from this publication is available from the lead author.

References

Ancell B, Hakim GJ. 2007. Comparing adjoint- and ensemble-sensitivity analysis with applications to observation targeting. *Mon. Weather Rev.* **135**: 4117–4134.

Baldwin ME, Lakshmivarahan S, Kain JS. 2001. Verification of mesoscale features in NWP models. In *Preprints, Ninth Conference on Mesoscale Processes,* Fort Lauderdale, FL: 255–258. American Meteorological Society: Boston, MA.

Bowler NE, Arribas A, Mylne KR, Robertson KB, Beare SE. 2008. The MOGREPS short-range ensemble prediction system. *Q. J. R. Meteorol. Soc.* **134**: 703–722.

Brown A, Milton S, Cullen MJP, Golding B, Mitchell J, Shelly A. 2012. Unified modeling and prediction of weather and climate. *Bull. Am. Meteorol. Soc.* **93**: 1865–1877.

Clark AJ, Gallus WA, Xue M, Kong F. 2009. A comparison of precipitation forecast skill between small convection-allowing and large convection-parameterizing ensembles. *Weather and Forecasting* **24**: 1121–1140.

Cosma S, Richard E, Miniscloux F. 2002. The role of small-scale orographic features in the spatial distribution of precipitation. *Q. J. R. Meteorol. Soc.* **128**: 75–92.

Crook NA, Tucker DF. 2005. Flow over heated terrain. Part I: Linear theory and idealized numerical simulations. *Mon. Weather Rev.* **133**: 2552–2564.

Davies T, Cullen MJP, Malcolm AJ, Hawson MH, Staniforth A, White AA, Wood N. 2005. A new dynamical core for the Met Office's global and regional modelling of the atmosphere. *Q. J. R. Meteorol. Soc.* **131**: 1759–1782.

Doswell CA, Brooks HE, Maddox RA. 1996. Flash flood forecasting: An ingredients-based methodology. *Weather and Forecasting* **11**: 560–581.

Edwards JM, Slingo A. 1996. Studies with a flexible new radiation code. I: Choosing a configuration for a large-scale model. *Q. J. R. Meteorol. Soc.* **122**: 689–719.

Fuhrer O, Schär C. 2007. Dynamics of orographically triggered banded convection in sheared moist orographic flows. *J. Atmos. Sci.* **64**: 3542–3561.

Godart A, Anquetin S, Leblois E, Creutin J. 2011. The contribution of orographically driven banded precipitation to the rainfall climatology of a Mediterranean region. *J. Appl. Meteorol. Climatol.* **50**: 2235–2246.

Golding B. 2005. The Boscastle flood: Meteorological analysis of the conditions leading to the flooding on 16 August 2004. *Weather* **60**: 230–235.

Gregory D, Rowntree PR. 1990. A mass flux convection scheme with representation of cloud ensemble characteristics and stability dependent closure. *Mon. Weather Rev.* **118**: 1483–1506.

Hanley KE, Kirshbaum DJ, Belcher SE, Roberts NM, Leoncini G. 2011. Ensemble predictability of an isolated mountain thunderstorm in a high-resolution model. *Q. J. R. Meteorol. Soc.* **137**: 2124–2137.

Hanley KE, Kirshbaum DJ, Roberts NM, Leoncini G. 2013. Sensitivities of a squall line over central Europe in a convective-scale ensemble. *Mon. Weather Rev.* **141**: 112–133.

Harrison DL, Scovell RW, Kitchen M. 2009. High-resolution precipitation estimates for hydrological uses. *Proc. ICE –Water Manage.* **162**: 125–135.

Harrison DL, Norman K, Pierce C, Gaussiat N. 2012. Radar products for hydrological applications in the UK. *Proc. ICE –Water Manage.* **165**: 89–103.

Kendon EJ, Roberts NM, Senior CA, Roberts MJ. 2012. Realism of rainfall in a very high-resolution regional climate model. *J. Clim.* **25**: 5791–5806.

Kirshbaum DJ. 2013. On thermally forced circulations over heated terrain. *J. Atmos. Sci.* **70**: 1690–1709.

Kirshbaum DJ, Durran DR. 2005. Observations and modeling of banded orographic convection. *J. Atmos. Sci.* **62**: 1463–1479.

Kirshbaum DJ, Bryan GH, Rotunno R, Durran DR. 2007. The triggering of orographic rainbands by small-scale topography. *J. Atmos. Sci.* **64**: 1530–1549.

Langhans W, Gohm A, Zängl G. 2011. The orographic impact on patterns of embedded convection during the August 2005 Alpine flood. *Q. J. R. Meteorol. Soc.* **137**: 2092–2105.

Lean HW, Roberts NM, Clark PA, Morcrette C. 2009. The suprising role of orography in the initiation of an isolated thunderstorm in Southern England. *Mon. Weather Rev.* **137**: 3026–3046.

Lock AP, Brown AR, Bush MR, Martin GM, Smith RNB. 2000. A new boundary-layer mixing scheme. Part I: Scheme description and single-column model tests. *Mon. Weather Rev.* **128**: 3187–3199.

Mass C. 1981. Topographically forced convergence in western Washington state. *Mon. Weather Rev.* **109**: 1335–1347.

Mass CF, Ovens D, Westrick K, Colle BA. 2002. Does increasing horizontal resolution produce more skillful forecasts? *Bull. Am. Meteorol. Soc.* **83**: 407–430.

Miglietta MM, Rotunno R. 2009. Numerical simulations of conditionally unstable flows over a mountain ridge. *J. Atmos. Sci.* **66**: 1865–1888, doi: 10.1175/2009JAS2902.1.

Miniscloux F, Creutin JD, Anquetin S. 2001. Geostatistical analysis of orographic rainbands. *J. Appl. Meteorol.* **40**: 1835–1854.

Mittermaier M, Roberts N, Thompson SA. 2013. A long-term assessment of precipitation forecast skill using the fractions skill score. *Meteorol. Appl.* **20**: 176–186.

Reinecke PA, Durran DR. 2008. Estimating topographic blocking using a Froude number when the static stability is non-uniform. *J. Atmos. Sci.* **65**: 1035–1048.

Reisner JM, Smolarkiewicz PK. 1994. Thermally forced low Froude number flow past three-dimensional obstacles. *J. Atmos. Sci.* **51**: 117–133.

Roberts NM, Lean HW. 2008. Scale-selective verification of rainfall accumulations from high-resolution forecasts of convective events. *Mon. Weather Rev.* **136**: 78–97.

Roberts NM, Cole SJ, Forbes RM, Moore RJ, Boswell D. 2009. Use of high-resolution NWP rainfall and river flow forecasts for advance warning of the Carlisle flood, north-west England. *Meteorol. Appl.* **16**: 23–34.

Roebber PJ, Schultz DM, Colle BA, Stensrud DJ. 2004. Toward improved prediction: High-resolution and ensemble modeling systems in operations. *Weather and Forecasting* **19**: 936–949.

Schumacher RS, Schultz DM, Knox JA. 2010. Convective snowbands downstream of the Rocky Mountains in an environment with conditional, dry symmetric, and inertial instabilities. *Mon. Weather Rev.* **138**: 4416–4438.

Smagorinsky J. 1963. General circulation experiments with the primitive equations. *Mon. Weather Rev.* **91**: 99–164.

Smith RNB. 1990. A scheme for predicting layer clouds and their water content in a general circulation model. *Q. J. R. Meteorol. Soc.* **116**: 435–460.

Torn RD, Hakim GJ. 2008. Ensemble-based sensitivity analysis. *Mon. Weather Rev.* **136**: 663–677.

Vosper SB, Wells H, Brown AR. 2009. Accounting for non-uniform static stability in orographic drag parameterization. *Q. J. R. Meteorol. Soc.* **135**: 815–822, doi: 10.1002/qj.407.

Warren RA, Kirshbaum DJ, Plant RS, Lean HW. 2014. A 'Boscastle-type' quasi-stationary convective system over the UK Southwest peninsula. *Q. J. R. Meteorol. Soc.* **140**: 240–257, doi: 10.1002/qj.2124.

Wernli H, Paulat M, Hagen M, Frei C. 2008. SAL-A novel quantity measure for the verification of quantitative precipitation forecasts. *Mon. Weather Rev.* **136**: 4470–4487.

Wilson RW, Ballard SP. 1999. A microphysically based precipitation scheme for the UK Meteorological Office Unified Model. *Q. J. R. Meteorol. Soc.* **125**: 1607–1636.

Yoshizaki M, Kato T, Tanaka Y, Takayama H, Shoji Y, Seko H. 2000. Analytical and numerical study of the 26 June 1998 orographic rainband observed in Western Kyushu, Japan. *J. Meteorol. Soc. Jpn.* **78**: 835–856.

Yuter SE, Stark DA, Crouch JA, Payne MJ, Colle BA. 2011. The impact of varying environmental conditions on the spatial and temporal patterns of orographic precipitation over the Pacific Northwest near Portland, Oregon. *J. Hydrometeorol.* **12**: 329–351.

Zhang F, Odnis AM, Neilsen-Gammon JW. 2006. Mesoscale predictability of an extreme warm-season precipitation event. *Weather and Forecasting* **21**: 149–166.